Stability analysis of flow structures in hovering using robotic experiments and flow visualizations

Alejandro Marín-Navarro, Jorge Aguilar-Cabello, Luis Parras, Carlos del Pino
1: Universidad de Málaga, Escuela de Ingenierías Industriales, Campus de Teatinos, 29071, Málaga, Spain.
* Correspondent author: lparras@uma.es

Keywords: PIV, flapping wings, unsteady aerodynamics

ABSTRACT

We investigate the kinematics and stability of hovering flight making use of a robotic experimental device that simulate the movement of insects or birds. We carried out this analysis based on the characterization of this movement with flow visualizations and particle image velocimetry -PIV-. First, we characterized the kinematics of the robotic device inside water. Therefore, it has been verified that the robotic experiments follow the desired input signal precisely. Second, we give qualitative and quantitative information from the experimental tests as a function of frequency and angular amplitude. The kinematics of the hovering flight produces vortices that are stable or unstable around the rigid flat plate, as well as one transient regime that has been also found between these two latter states. Finally, dimensional velocity field plus associated vorticity have been characterized in these flow regimes through PIV measurements, and we also validated the reproducibility of experiment finding excellent agreement between different set of experiments.

1. Introduction

In the last years, the non-stationary aerodynamic study of flapping wings at low Reynolds numbers has acquired a great relevance due to the development of micro air vehicles (MVA), see the thorough revision given in Shyy et al. (2010) and the example given in Fig. 1. The traditional formulation can not predict the non-stationary aerodynamic forces of lift and thrust (or resistance) for large Reynolds numbers. Therefore, the mechanic formulation is much more complex, not only due to the non-stationary geometry but also due to the large variety of physical processes involved (Wang et al. 2013, Ya 2013, Birch et al. 2004, Bonfrey et al 2017, Dickinson et al. 1993, Lua et al. 2008). For this reason, it is demanded the use of sophisticated numerical tools for the resolution of the Navier-Stokes equations in moving meshes, as well as complex and sophisticated experimental techniques for the validation of theoretical and numerical results, see for instance Martín-Alcántara et al. (2015).

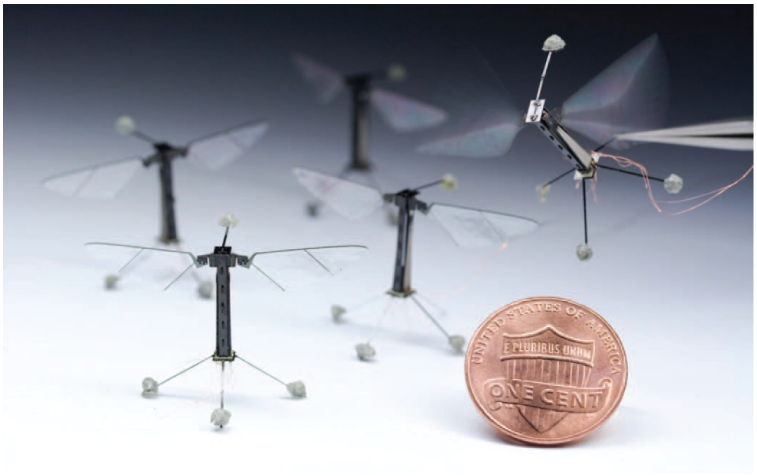

Fig. 1 Example of micro air vehicle extracted from reference Ya et al. (2013).

One robotic experimental setup has been designed and built to model a pair of dragonfly wings that allows several degrees of freedom. Also, this device will help to investigate the best configuration in terms of phase between wings, pitch angle, frequency or amplitude. Hence, this robotic experiment will give us a precise guide to select different configurations that would be simulated numerically. These simulations together with flow visualizations and PIV measurements will offer a better understanding of the fluid dynamic mechanisms produced by the optimal hovering flight. All the knowledge acquired from both experimental and numerical results will show potential improvements that must be applied to the micro air vehicles.

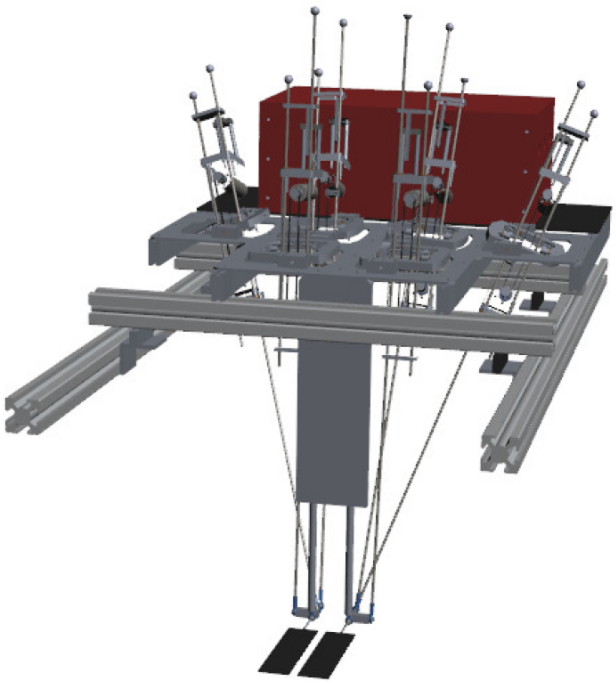

Fig. 2 3D schematic of the experimental setup.

2. Experimental setup

The present study has been carried out in the arrangement shown in Fig. 2 to reproduce different flight configurations. The device consists of six servomotors that follow precisely the movement of a rigid polycarbonate flat plate that has a chord of 30 mm, and it is 150 mm long in the span direction. These six servomotors provide six degrees of freedom (three degrees per wing) which will allow us to investigate the whole spatial scenario. Each servomotor has one encoder with 256 pulses per revolution and a reduction gear coupled with a relation of 326:1. The gear with 16 tooth type T2 (2 mm step) force the movement to another gear by means of a timing belt pulley that also transmit the motion to a rod. This rod is attached to one patella that is joint to the wing shaft. The final result is a particular spatial displacement of the wing . In Fig. 2 is also observed (i) the structure made of aluminum that is aligned within 0.1°, and (ii) the red box that contains the set of controllers which are connected to the computer and allow us the human-machine interaction. In this study, we use only one rigid polycarbonate plate as a first approximation to validate the system. Our kinematics follow a linear displacement for each shaft that moves the wing. The definition of displacement angles for the wing is shown in Fig. 3. The shafts which displace the servomotors are used as the necessary points to define the kinematics and they are represented in the schematic depicted in Fig. 4. The position of each servomotor to move one wing is given by the modulus of vectors $\overrightarrow{RM_iM_i}$. First, vectors $\overrightarrow{R_1M_i}$ are calculated as follows:

$$\overrightarrow{R_1M_2} = [-B\cos\Theta_1\sin\phi_1, -B\sin\Theta_1\sin\phi_1, -B\cos\phi_1], \quad (1)$$

$$\overrightarrow{R_1M_3} = [-C\cos\Theta_1\sin\phi_1, -C\sin\Theta_1\sin\phi_1, -C\cos\phi_1]. \quad (2)$$

The computation of the vector $\overrightarrow{R_1M_1}$ is more complex due to the presence of the patella M_1 that is not on the wing shaft, so it requires several steps. First, the vector from R_1 to the anchorage point on the wing shaft can be expressed as:

$$\overrightarrow{R_1M_1'} = [-A\cos\Theta_1\sin\phi_1, -A\sin\Theta_1\sin\phi_1, C\cos\phi_1]. \quad (3)$$

Second, we calculate the vector that joins the anchorage point with the point that would be on the patella M_1 in the case of being both perpendicular or horizontal. This point will be called M_1'' and it follows the expression:

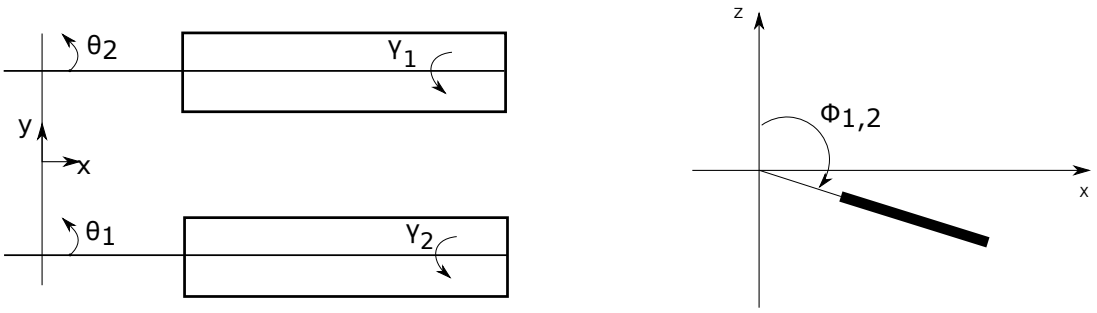

Fig. 3 2D schematic of the coordinate system.

$$\overrightarrow{M_1{}'M_1{}''} = [-D\sin\Theta_1, D\cos\Theta_1, 0]. \quad (4)$$

Third, the vector $\overrightarrow{M_1{}'M_1}$ stems from the rotation of vector $\overrightarrow{M_1{}'M_1{}''}$ to its real position as follows:

$$\overrightarrow{M_1{}'M_1} = \overrightarrow{M_1{}'M_1{}''} \cdot R. \quad (5)$$

where R is the rotation matrix.

Following these three calculations, the final vector $\overrightarrow{R_1M_1}$ can be obtained using the definition

$$\overrightarrow{R_1M_1} = \overrightarrow{R_1M_1{}'} + \overrightarrow{M_1{}'M_1}. \quad (6)$$

Finally, and using all data have been obtained from the developments described above, the distance for each servomotor can be calculated by the modulus of each vector $\overrightarrow{RM_\iota M_\iota}$, where

$$\overrightarrow{RM_1M_1} = -\overrightarrow{RM_1} + \overrightarrow{R_1} + \overrightarrow{R_1M_1}, \quad (7)$$

$$\overrightarrow{R_1M_2M_2} = \overrightarrow{R_1} + \overrightarrow{R_1M_2}, \quad (8)$$

$$\overrightarrow{R_1M_3M_3} = \overrightarrow{R_1} + \overrightarrow{R_1M_3}. \quad (9)$$

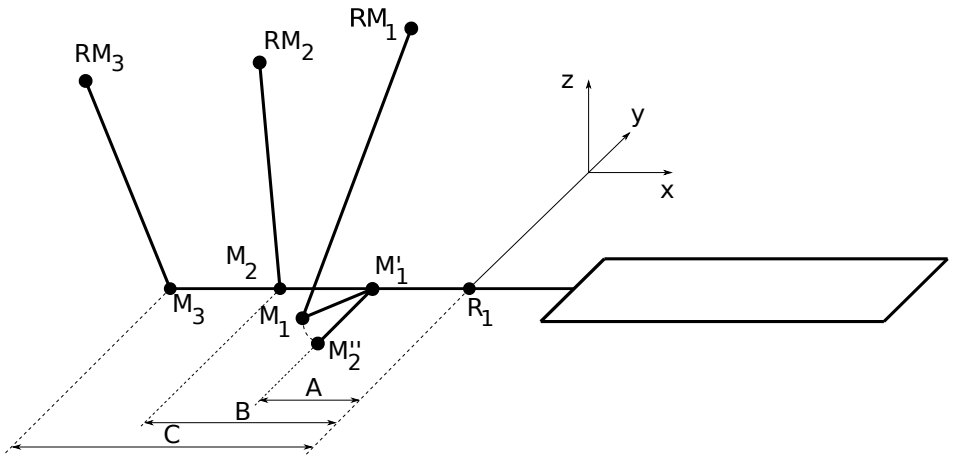

Fig. 4 Representation of schaft and patellas for one wing of the robotic experiment.

2. Visual analysis

Two experimental methods have been applied to obtain information from the structures produced in the wing dynamics: (i) flow visualizations and (ii) PIV. As mentioned above, the experimental setup has been introduced in a water tank, and different devices have been provided to perform flow visualization and PIV such as optics, lens, green lasers (500 mW or 2000 mW power supply) and a high-speed video camera (up to 60000 fps, but only 125 fps were required), as well as the use of retarder painting with Rhodamine.

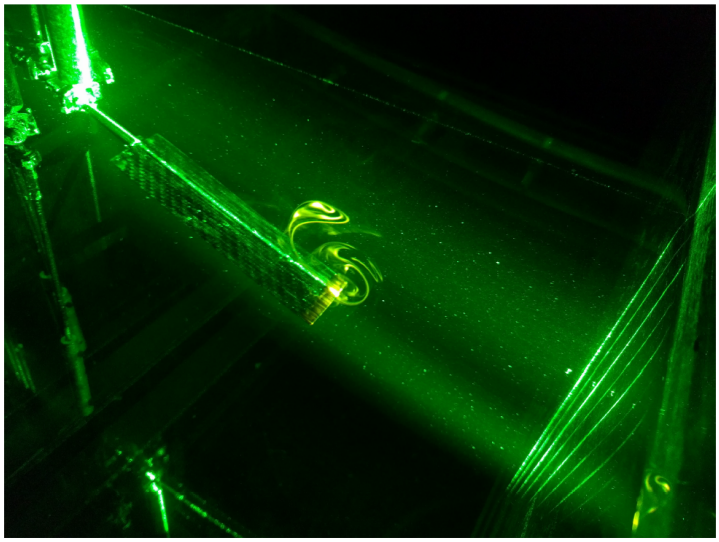

Fig. 5 Flow visualization of the wing together with the laser plane and streaklines formed in hovering flight.

2.1 Flow visualizations

Flow visualizations consist of illuminating the area of interest with a laser (x, z)-plane, where a mixture of acrylic retarder with rhodamine has been applied to the tip of the rigid at plate. This mixture is diluted slowly in the medium, so during the movement of the wing some particles of this mixture are released into the water, thus highlighting the flow patterns that are observed visually. The high-speed camera records these patterns, so this information is analyzed to distinguish different flow structures during the movement in several wing cycles. One snapshot of the recording process is shown in Fig. 5, in which it is observed how the laser plane is aligned to the axial direction of the wing, whereas it is perpendicular to the high-speed camera. This type

of technique is considered non-intrusive since the density of the mixture is similar to the water.

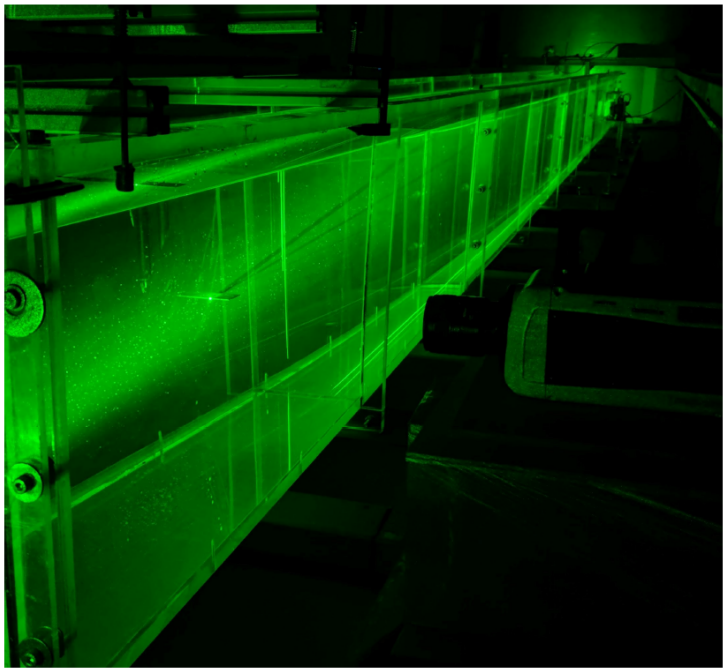

Fig. 6 PIV setup for measurements in the (y, z) –plane: laser plane and high speed camera.

2.2 Particle image velocimetry.

2D-PIV (Particle Image Velocimetry) allows us to determine the velocity field in a laser in both (x, z) and (y, z)-planes. For instance, the arrangement to perform PIV in the (y, z)-plane is shown in Fig. 6. It is observed how in this case the laser plane is perpendicular to the axial direction of the wing . In this case, the information of the velocity field is relevant to complement our observations performing 2D flow visualizations since it allows us to build a three dimensional perspective [(x, z) and (y, z)-planes].

3. Results

In this section, different results obtained from the two techniques described above will be shown and explained. Our main objective is to consider the stability of hovering flight after the application of flow visualizations and PIV. The variables that correspond to different cases of study are presented in Fig. 7 where we show a 3D schematic of the angles that define the different movements: ϕ is the pitch angle, Θ is the yaw angle, and γ is the roll angle. Remember that only the case of $\Theta = \gamma = 0$ has been considered in this work.

Table I shows the cases os study carried out together with the figures associated with each case.

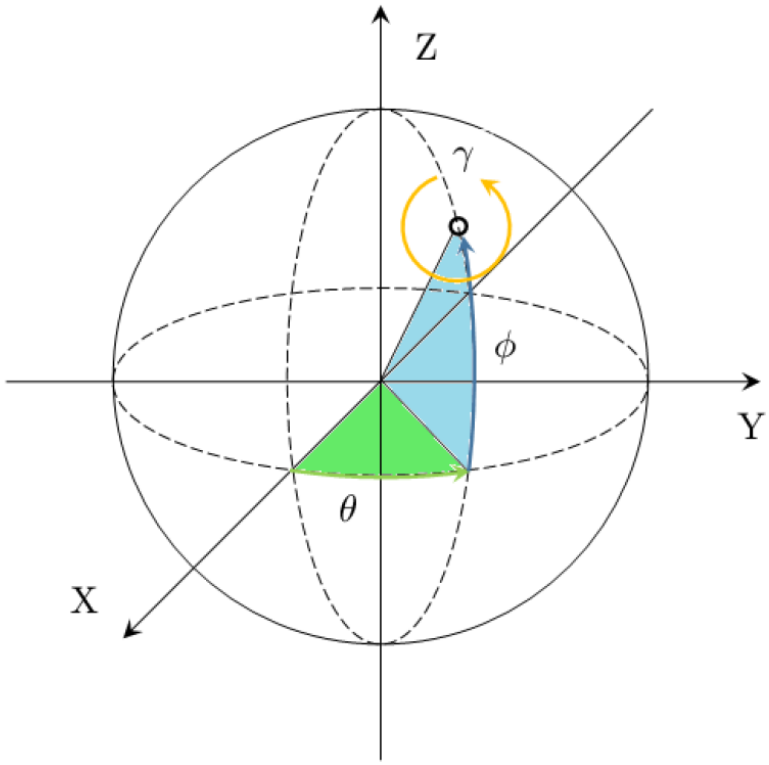

Fig. 7 Spatial definition of the spherical coordinate system.

	Figures	$f(Hz)$	$\phi(º)$
Visualization Figures	Fig. 8	0.05	5
	Fig. 9	0.05	10
	Fig. 10	0.1	10
PIV Figures	Fig. 12	0.05	10
	Fig. 13	0.1	5
	Fig. 14	0.05	10
	Fig. 15	0.2	5

Table I. Cases of study.

3.1 Stability.

The stability analysis of the vortices are based on the study of streaklines. These lines are defined as the lines formed by all the fluid particles that at certain time passed through one point x_0. Also, these streaklines enclose information of the fluid flow in the previous instant of time. Since the movement is non-stationary, these streaklines do not match with any of the trajectories of particles, nor with any of the pathlines that pass through that point at a particular instant time. This fact represents the main difficulty involved in the interpretation of visualizations. The parameters to be taken into account in flow visualizations are the frequency and the angular amplitude. Several tests were carried out for movements in the (x, z)-plane in the hovering flight configuration to characterize the stability of the flow. For this reason, we distinguish between the following structures (according to one specific criterion):

- Fully stable flow: streaklines are stable showing perfectly the shape of the vortices (see, for instance, Fig. 8).

- Instability by shear stress inside the vortex: The internal part of vortices remain unstable, but their bounds are stable and well-defined (see the example given in Fig. 9).

- Fully unstable flow: The streaklines do not present stability, even enhancing vortex breakdown (as shown in Fig. 10).

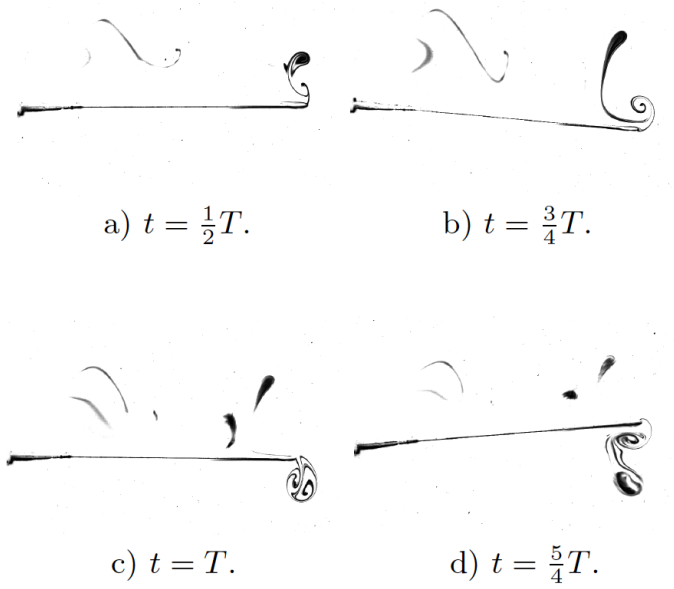

Fig. 8 Visualization of hovering flight of angular amplitude $\phi = 5°$ and $f = 0.05\ Hz$.

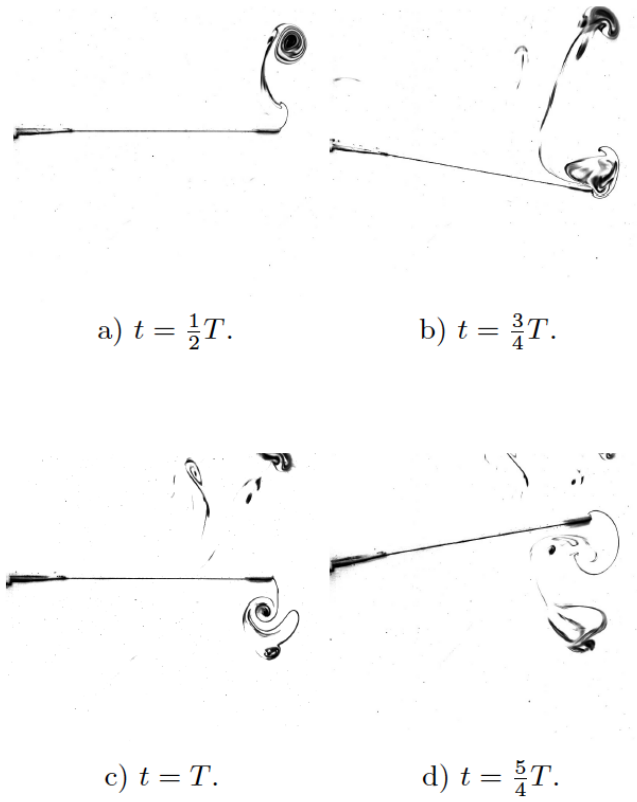

Fig. 9 Visualization of hovering flight of angular amplitude $\phi = 10°$ and $f = 0.05\ Hz$.

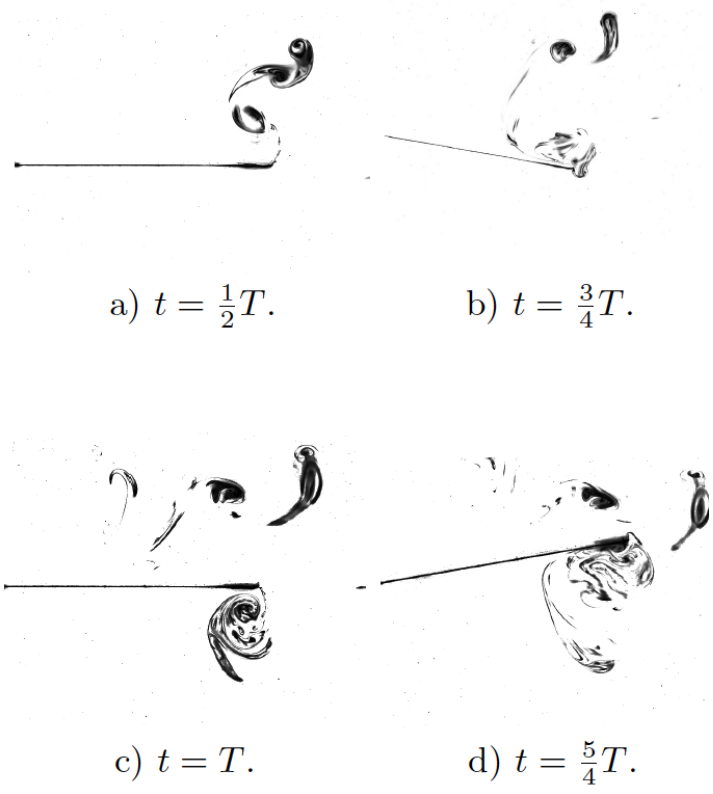

Fig. 10 Visualization of hovering flight of angular amplitude $\phi = 10°$ and $f = 0.1\ Hz$.

Once the different structures have been differentiated according to their typology (Stable, Transient or Unstable), several tests have been carried out for different values of angular amplitude and frequency. The results are shown in Fig. 11, where all experimental data from flow visualization has been represented: stable (red circles), unstable (blue crosses) and transient regime by shear stress (orange crosses). We observe that the frequency increases as the angular amplitude decreases for both stable and unstable cases. In addition, the frequency tends to a constant value for the highest angular amplitudes considered.

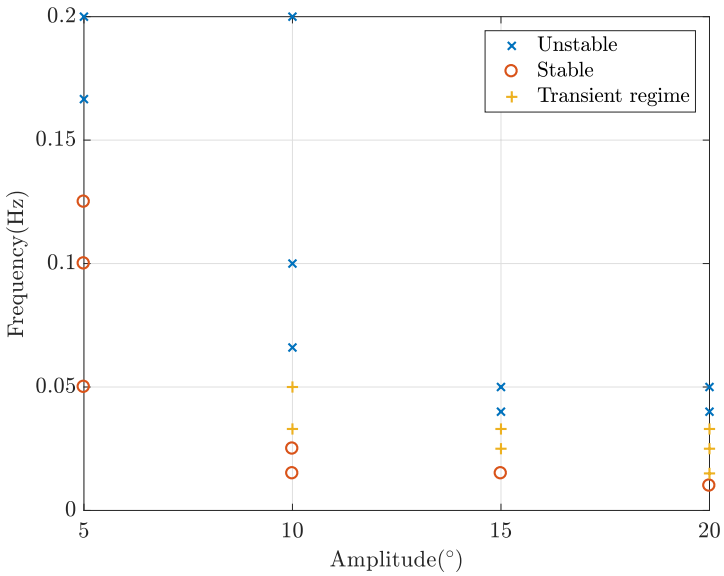

Fig. 11 Characterization of the flow structure for different setpoint values in a hovering flight configuration .

3.2 PIV

As mentioned above, the results obtained after PIV analysis are the dimensional velocity field plus associated vorticity. We have verified the reproducibility of the experiments, for which three cases have been tested with the same values as shown in Fig. 12. It can be observed that the shape of the vortex is quite similar in these three cases, with positive vorticity values (counterclockwise) and also presenting an excellent agreement regarding the velocity field.

Also, the values of maximum and minimum vorticity have been depicted for three experiments for $\phi = 5°$ and $f = 0.1\,Hz$ in Fig. 13. It can be observed how the vorticity presents periodic values, after a starting process. Also, it can be distinguished different types of structures previously identified for the stability analysis of the vortices, as shown in Fig. 14: there is a stable

vortex with a negative vorticity value (clockwise) during the upward movement in the snapshot (a), whereas the instability occurs by shear stress when the wing begins to rise, and the vortex with negative vorticity value (cold tone) forms a mixture with the vortex in the descent movement (warm tone) in the image (b); finally, image (c) shows how the existing instability promotes the vortex disintegration.

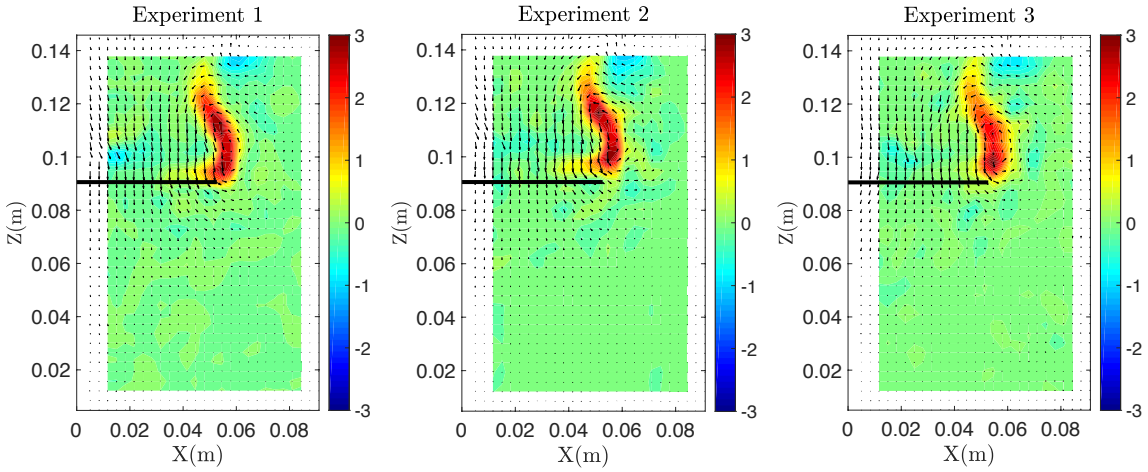

Fig. 12 Dimensional velocity field and vorticity for three different experiments with the same setpoint values ($\phi = 10°$ and $f = 0.05\ Hz$) at $t = T/2$ in hovering flight.

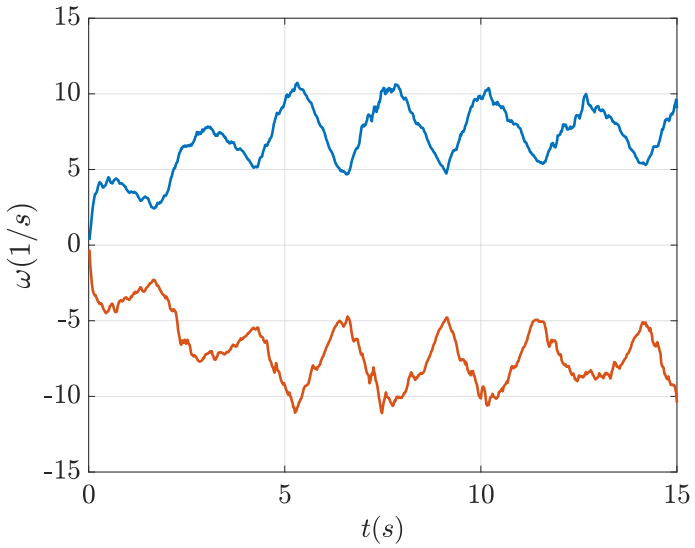

Fig. 13 Maximum and mínimum vorticity values for parameters values $\phi = 5°$ and $f = 0.1\ Hz$ in six cicles of hovering flight.

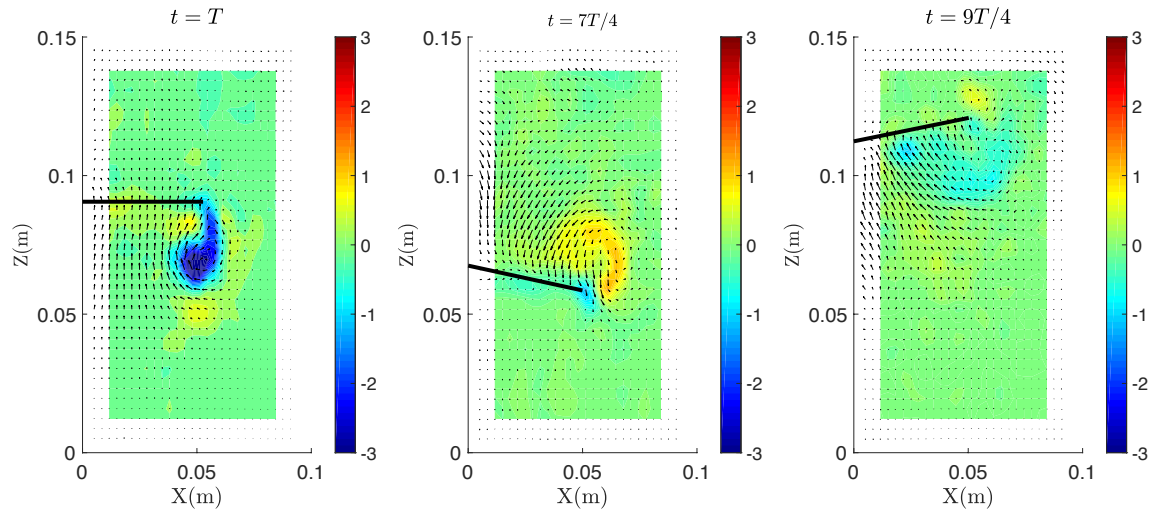

Fig. 14 Identification of unstable structures using PIV: stable state (a), transient regime (b) and unstable case for values of $\phi = 10°$ and $f = 0.05\ Hz$.

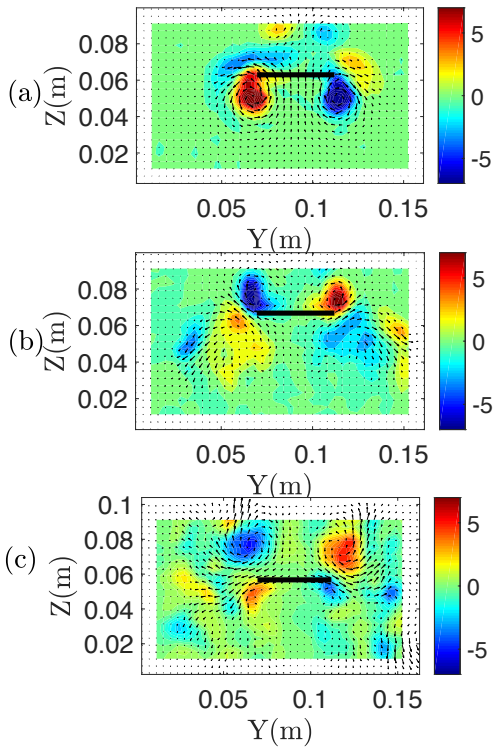

Fig. 15 Velocity and vorticity in hovering flight configuration with $\phi = 5°$ and $f = 0.2\ Hz$ at different instants of time: (a) $t = T$, (b) $t = 7T/5$, (c) $t = 9T/5$

Finally, the result of the velocity field and the vorticity is shown in Fig. 15 for hovering flight in the (y, z)-plane. The values of vorticity correspond to those observed in Fig. 13, thus showing the formation of vortices on both sides of the wing present similar magnitudes and opposite direction of rotation. This fact proves the symmetry of the fluid flow in the (y, z)-plane although the flow presents a transient regime.

4. Conclusions

We investigate the kinematics and stability of hovering flight by the use of a robotic experimental device. We provide the stability diagram as a function of frequency and angular amplitude and we observe that the frequency increases as the angular amplitude decreases for both stable and unstable cases. In addition, the frequency tends to a constant value for the highest angular amplitudes considered.

This work has been supported by the Ministerio de Economía y Competitividad (Spain) Grant No. DPI2013-40479-P and DPI2016-76151-C2-1-R and Junta de Andalucía Grant No. P11-TEP-7776.

5. Bibliography

Birch J.M., Dickson W. B., Dickinson M. H. (2004). Force production and flow structure of the leading edge vortex on flapping wings at high and low Reynolds numbers. The Journal of Experimental Biology 207, 1063-1072.

Bomphrey R. J., Nakata T., Phillips N. and Walker S. M. (2017). Smart wing rotation and trailing-edge vortices enable high frequency mosquito flight Nature 21727.

Dickinson M. H. and Gtz K. G. (1993). Unsteady aerodynamic performance of model wings at low Reynolds numbers, The Journal of Experimental Biology, 174, 45-64.

Lua, K. B., Lim T. T. and Yeo, K. S. (2008). Aerodynamic forces and flow fields of a two-dimensional hovering wing, Experiments in Fluids, 45: 1047-1065.

Martín-Alcántara, A. and Fernandez-Feria R. and Sanmiguel-Rojas E. (2015). Vortex flow structures and interactions for the optimum thrust effciency of a heaving airfoil at different mean angles of attack, Physics of Fluids, 2015.

Mueller T. J. (2001). Fixed and flapping wing aerodynamics for micro air vehicle applications, Progress in Astronautics and Aeronautics (195), AIAA, Reston.

Raffel M., Willert C. E., Werely S. T. and Kompenhans J. (2007). Particle Image Velocimetry. A Practical Guide, Springer Verlag.

Shyy W., Aono H., Chimakurtthi S. K., Trizila P., Kang C. K., Cesnik C. E. S. and Liu, H. (2010) Recent progress in apping wing aerodynamics and aeroelasticity, Progress in Aerospace Sciences, 46.

Ya K. Y., Chirarattananon P., Fuller S. B., Wood, R. J. (2013) Controlled Flight of a Biologically Inspired, Insect-Scale, Science, 340, 603-607.

Wang S., Zhang X., He and Liu, T. (2013) A lift formula applied to low-Reynolds-number unsteady ows, Phys. Fluids, 25, 093605.